Observation of Electron-Temperature Fluctuations Triggered by Supersonic Gas Puffing in the LHD

Akiyoshi MURAKAMI, Junichi MIYAZAWA[1)], Koji YASUI[1)], Takanori MURASE[1)], Naoki TAMURA[1)], Hayato TSUCHIYA[1)], Yoshiro NARUSHIMA[1)], Tomohiro MORISAKI[1)], Ryuichi SAKAMOTO[1)], Hiroshi YAMADA[1)] and LHD Experiment Group[1)]

The Graduate University for Advanced Studies, 322-6 Oroshi-cho, Toki 509-5292, Japan
[1)]*National Institute for Fusion Science, 322-6 Oroshi-cho, Toki 509-5292, Japan*

(Received 4 April 2011 / Accepted 9 August 2011)

Non-local transport and electron temperature fluctuations triggered by supersonic gas puffing (SSGP) in high-temperature helical plasmas in the Large Helical Device (LHD) are reported. After a short-pulse SSGP, the core electron temperature increased while the edge electron temperature decreased. SSGP triggered a longer core temperature increase than that triggered by a small impurity pellet injection. The temperature profile, which was relatively flat inside the half minor radius before SSGP, became parabolic after non-local transport was triggered. Fluctuations were excited in the electron temperature signals around the half minor radius. The frequency of these fluctuations increased from ~ 400 Hz to ~ 1 kHz within ~ 0.1 s and the amplitude decreased correspondingly. The temperature fluctuations inside and outside of the half minor radius had opposite phases. Magnetic fluctuations resonating near the half minor radius were observed simultaneously with the electron temperature fluctuations.

Keywords: fueling method, supersonic gas puffing, electron temperature fluctuation, non-local transport phenomenon, heliotron

DOI: 10.1585/pfr.6.1402135

1. Introduction

Non-diffusive heat transport, which cannot be explained by ordinary local diffusion, has been observed in magnetically confined toroidal plasmas. Many kinds of peculiar non-local transport phenomena have been reported by both tokamak and helical experiments [1–6]. For example, an edge cooling perturbation can cause the core electron temperature to start increasing under certain conditions. In the Large Helical Device (LHD), non-local transport is triggered by a small hydrogen ice pellet injection, a small impurity pellet (tracer-encapsulated solid pellet, TESPEL) injection, or Ar gas puffing [4, 5].

A supersonic gas puffing (SSGP) system has been installed in the LHD since 2009. SSGP is able to generate convergent gas flow, and short-pulse SSGP causes a rapid density increase, like that observed in pellet injection experiments. In SSGP, the number of fueled atoms, the timing, and the number of injections are continuously variable. This flexibility makes SSGP a valuable tool for studying non-local transport. In this paper, experimental results on non-local transport triggered by SSGP are reported.

2. Supersonic Gas Puffing

SSGP is being developed as a new fueling method for the LHD [7, 8]. In SSGP, high-pressure gas is ejected through a fast solenoid valve equipped with a Laval nozzle. A solenoid valve from the Parker-Hannifin Pulse Valve Series 99B08, with an available backing pressure as high as ~ 8 MPa, is used in the SSGP system. This pressure is much higher than that of typical piezo-electric valves (~ 0.1 MPa) used in conventional gas puffing. The solenoid valve can be operated with a short pulse of ~ 100 μs. This is also much faster compared with that of typical piezo-electric valves. A Laval nozzle of 300-μm throat diameter is placed at the exit of the solenoid valve, and it plays an important role in generating the convergent gas flow. In the LHD, the distance from the Laval nozzle to the plasma is ~ 4 m.

3. Non-Local Transport and Electron Temperature Fluctuations Triggered by SSGP

Figures 1 (a) and 1 (b) show the time evolution of the electron temperature T_e, measured by an electron cyclotron emission (ECE) radiometer, for various values of the normalized minor radius ρ, where a TESPEL was injected at

author's e-mail: murakami.akiyoshi@LHD.nifs.ac.jp

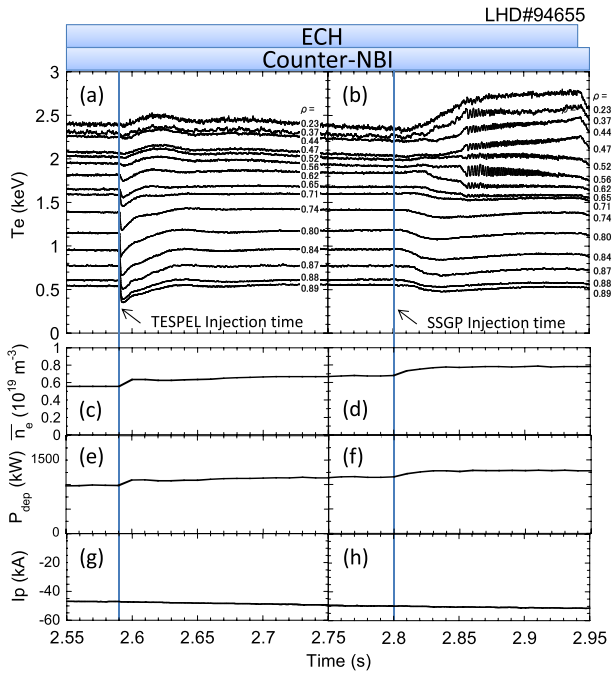

Fig. 1 Temporal evolutions of (a) and (b) the electron temperature at different normalized minor radii, (c) and (d) the line-averaged density, (e) and (f) the NBI deposition power P_{dep}, and (g) and (h) the plasma current. Non-local transport phenomena are triggered after the TESPEL injection at t = 2.59 s and SSGP at t = 2.80 s.

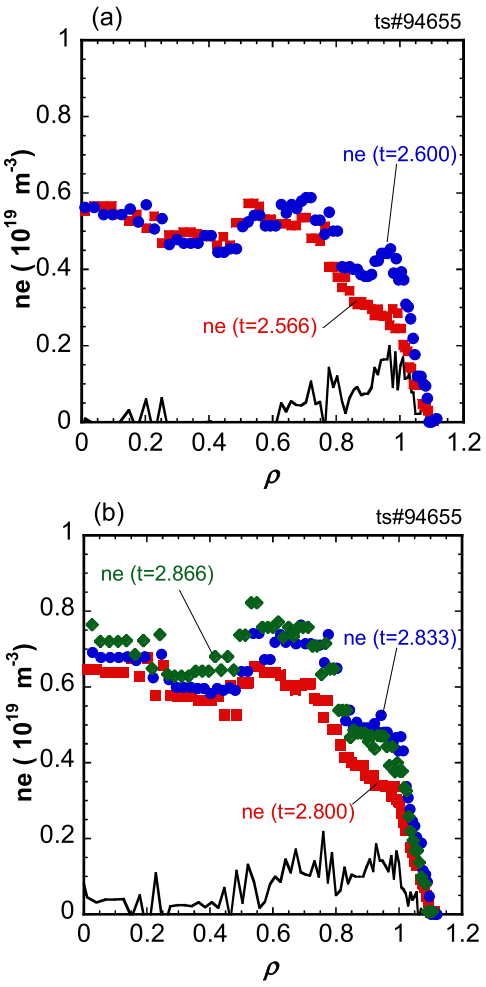

Fig. 2 Radial profiles of the electron density (a) before (t = 2.566 s) and after (t = 2.600 s) the TESPEL injection, and (b) before (t = 2.800 s) and after (t = 2.833 s) SSGP. The profile of t = 2.866 s is that with the temperature fluctuation. Solid lines in Figures (a) and (b) denote the difference between before and after injection.

t = 2.59 s and SSGP was injected at t = 2.80 s with a pulse length of 200 μs. The pulse length was shorter than that of SMBI, which had a pulse length of 3 ms and a backing pressure of 0.5 MPa and triggered non-local transport phenomena in the HL-2A tokamak [5]. In case of SSGP for this experiment, the working gas was hydrogen and the backing pressure was 1.2 MPa. SSGP is expected to generate more convergent and shorter-pulse gas flow compared with SMBI. The supplied particle number was estimated to be 2.2×10^{19} particles for the TESPEL injection and 2.4×10^{20} particles for SSGP. The target plasma was produced by electron cyclotron heating (ECH) of $\sim$ 0.8 MW and neutral beam injection (NBI) of $\sim$ 1.4 MW in the counter direction. The radial absorbed position of ECH power is estimated to be $\rho \sim 0.2$ from calculations of the the vacuum magnetic surface. The magnetic field strength on the magnetic axis was 2.85 T. The major and minor radii of the plasma were 3.6 m and 0.6 m, respectively.

Figures 1 (c) and 1 (d) show temporal evolutions of the line-averaged electron density $\bar{n}_e$. Figures 1 (e) and 1 (f) show the NBI deposition power P_{dep}, which is estimated by subtracting the shine-through power from the port-through power. Figures 1 (g) and 1 (h) show the plasma current. Figure 1 (a) shows non-local transport triggered by the TESPEL injection at t = 2.59 s. The line-averaged electron density increased by 0.1×10^{19} m^{-3} after SSGP. Then, the electron temperature increased in the core region while it decreased in the edge region, thus exhibiting non-local transport. Temporal evolutions of the line-averaged electron density and the plasma current were similar for both the TESPEL injection and SSGP. The profiles of ι are presumed to be unchanged at the time of the TESPEL injection and SSGP. The plasma current was ~ -50 kA in both cases.

Figure 2 shows radial profiles of the electron density measured by a YAG Thomson scattering system before (t = 2.566 s) and after (t = 2.600 s) the TESPEL injection (Fig. 2 (a)), and before (t = 2.800 s) and after (t = 2.833 s) SSGP (Fig. 2 (b)). Solid lines in Figs. 2 (a) and 2 (b) denote the density difference between before and after injection. Radial positions of notable increase in the electron density profile are $\rho \sim 0.8$ and $\rho \sim 0.6$ for the TESPEL injection and SSGP, respectively. In both cases, peaks in the radial profile after injection at $\rho > 0.8$ were observed. The peak of the density increase indicates that the supplied

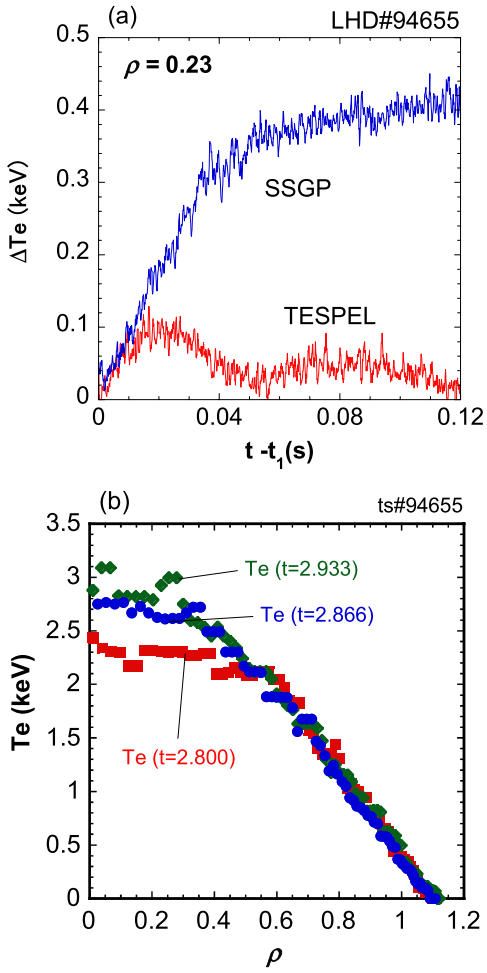

Fig. 3 (a) Temporal evolution of the electron temperature at $\rho = 0.23$ (t_1 in the figure is the time when the electron temperature started to increase). (b) Radial profiles of the electron temperature before ($t = 2.800$ s) and after ($t = 2.866$ s) SSGP. The profile of $t = 2.933$ s is that with the electron temperature fluctuation.

particles were mainly ionized at $\rho \sim 0.8$. According to the time evolutions of the electron density profiles, the peak for the TESPEL injection decreased in $\sim$ 40 ms, but the peak for SSGP was maintained for $\sim$ 80 ms. In addition, there is another peak in the electron density profile after SSGP at $\rho \sim 0.6$. This peak was maintained during this phenomenon. The radial position of the particle deposition estimated from the decrease in the electron temperature at various normalized minor radii measured by ECE is $\rho = 0.6 - 0.9$ for the TESPLE injection and $\rho = 0.8 - 0.9$ for SSGP (Figs. 1 (a) and 1 (b), respectively). Indeed, the penetration depth evaluated from ablation signals from the TESPEL injection is $\rho \sim 0.8$. The core density was not affected by the TESPEL injection. This is a typical characteristic of non-local transport phenomena. In contrast, the core density was increased by SSGP. This different effect on the core density is caused by the difference in supplied particle number between the TESPEL injection and SSGP.

In the LHD, non-local transport phenomena triggered by Ar gas puffing were also observed [5]. For Ar gas puffing, the delay time, which corresponds to the time from injection to core electron temperature increase, is longer than that for the TESPEL injection. The delay time for Ar gas puffing was estimated to be 50 ms. In this experiment, the delay time for SSGP was $\sim$ 10 ms, which is longer than that for the TESPEL injection. With regard to the plasma delay time, SSGP has intermediate properties between Ar gas puffing and TESPEL injection.

Figure 3 (a) shows the temporal evolutions of the electron temperature at $\rho = 0.23$ for both the TESPEL injection and SSGP. At $t - t_1 = 0 - 0.01$ s, where t_1 denotes the time when the electron temperature started to increase, the increase rates of the electron temperature are similar in both cases. However, SSGP created a longer temperature increase than the TESPEL injection. The reason for this is not understood yet. However, the increment of the electron temperature depends on the ECH power and the electron density, as reported by a previous study [4].

Figure 3 (b) shows the radial profiles of the electron temperature before ($t = 2.800$ s) and after ($t = 2.866$ s) SSGP. The central electron temperature increased from $\sim$ 2.3 to $\sim$ 3 keV after SSGP, while the edge electron temperature remained unchanged.

Fluctuations were observed in the electron temperature around $\rho \sim 0.5$ at $t = 2.86 - 2.93$ s in this discharge (See Fig. 1). The frequency of the fluctuations increased from $\sim$ 400 Hz to $\sim$ 1 kHz, while the amplitude decreased. Figure 4 (a) shows enlarged waveforms of the electron temperature fluctuations, and Fig. 4 (b) shows the radial profile of the rate of change in the electron temperature. As can be seen in this figure, the temperature fluctuations inside and outside of $\rho \sim 0.5$ had opposite phases. In other words, the radial gradient of the electron temperature at $\rho \sim 0.5$ repeatedly became steep and mild.

Noted that no significant confinement degradation due to this electron temperature fluctuation was recognized. Indeed, as shown in Fig. 3 (b), the electron temperature profile at $t = 2.866$ s, where the electron temperature fluctuation was observed, was similar to that at $t = 2.933$ s, where the temperature fluctuation was negligibly small.

4. Rotating Magnetic Structure and the Temperature Fluctuation

Magnetic fluctuations of poloidal mode number $m = 2$ were also observed with the electron temperature fluctuations. The poloidal rotation of these magnetic fluctuations, measured by saddle loops set at different poloidal angles, is shown in Fig. 5. The mode structure propagated in the ion-diamagnetic direction. The rotation frequency and amplitude of the magnetic fluctuations showed similar characteristics to those of the electron temperature fluctuations: the frequency increased from $\sim$ 400 Hz to $\sim$ 1 kHz and the amplitude decreased correspondingly. This corre-

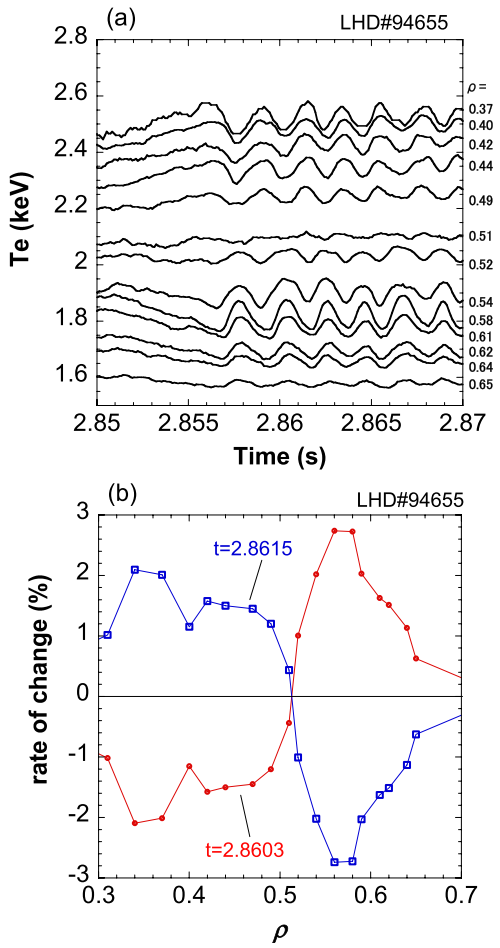

Fig. 4 (a) Enlarged waveforms of the electron temperature at $\rho = 0.37 - 0.65$. (b) Radial profile of the rate of change of the electron temperature. The phase of the electron temperature fluctuation inside $\rho \sim 0.5$ is opposite to that outside $\rho \sim 0.5$.

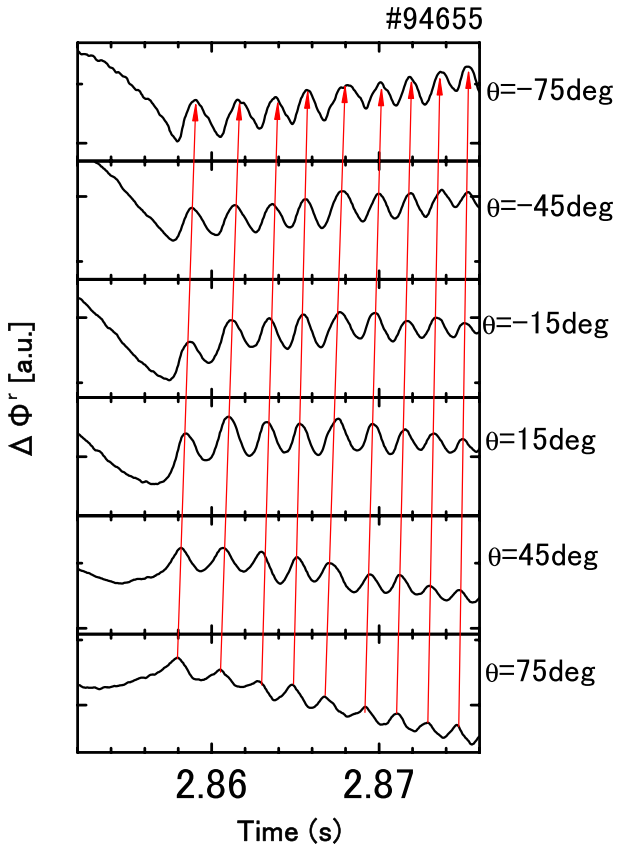

Fig. 5 Poloidal propagation of the radial component of the magnetic field measured by saddle loops set at various poloidal angles in the same discharge shown in Fig. 1. A coherent structure of poloidal mode number $m = 2$ is propagating in the ion-diamagnetic direction.

lation suggests that the electron temperature fluctuations were caused by the rotating magnetic mode structure. In the magnetic configuration used in this study, a rational surface of $m/n = 2/1$, where n is the toroidal mode number, is located at $\rho \sim 0.5$, assuming a vacuum magnetic surface. As was discussed in the previous section, the radial gradient of the electron temperature at $\rho \sim 0.5$ repeatedly became steep and mild (Fig. 4). In the LHD, it has been frequently observed that $m/n = 2/1$ magnetic fluctuations can cause local flattening in the electron temperature profile at its resonant position [9]. It is also possible to generate this flattening artificially using resonant magnetic perturbation coils placed in the LHD [10]. If the $m/n = 2/1$ magnetic island rotates, the temperature gradient at $\rho \sim 0.5$ may become steep (or mild) as the X-point (or O-point) of the island passes by the line of sight of the measurement. The magnetic intensities of these fluctuations were one order lower than that of typical $m/n = 2/1$ magnetic islands observed in the LHD. The width of the assumed magnetic islands is estimated to be less than 1 cm from the magnetic intensities. Therefore, local flattening is not obvious at $\rho \sim 0.5$ in the temperature profile shown in Fig. 4 (b). When these magnetic fluctuations disappeared, the amplitude and width of the magnetic islands decreased. According to these observations, a rotating $m/n = 2/1$ magnetic island is the possible cause of the electron temperature fluctuations observed in the non-local transport phenomenon triggered by SSGP.

5. Summary and Discussion

Non-local transport phenomenon triggered by short-pulse SSGP in the LHD was reported. SSGP triggered a longer temperature increase than that triggered by the TESPEL injection. Electron temperature fluctuations were observed around $\rho \sim 0.5$ after the core temperature increased. The frequency of the fluctuations increased and their amplitude decreased within 0.1 s. A rotating magnetic structure with $m = 2$ suggests that a rotating $m/n = 2/1$ magnetic island is the cause of these electron temperature fluctuations.

A similar correlation between electron temperature fluctuations and a rotating $m/n = 2/1$ magnetic island was

reported in JT-60U [11], where neoclassical tearing modes (NTMs) cause magnetic island formation. Characteristics of NTMs in helical plasmas and their role in non-local transport phenomena are, however, not yet understood and remain for future studies.

Acknowledgments

The authors would like to thank all the members of the LHD Experiment Group. This work has been financially supported by the Ministry of Education, Sports, Culture, Science and Technology, Grants-in-Aid for Scientific Research (S) 20226018 and NIFS09ULFF006.

[1] K.W. Gentle *et al*., Phys. Plasma **2**, 2292 (1995).
[2] F. Ryter *et al*., Nucl. Fusion **40**, 1917 (2000).
[3] M.W. Kissick *et al*., Nucl. Fusion **36**, 1691 (1996).
[4] N. Tamura *et al*., Nucl. Fusion **47**, 449 (2007).
[5] N. Tamura *et al*., Journal of Physics Conference Series **123**, 012023 (2008).
[6] H.J. Sun *et al*., Plasma Phys. Control. Fusion **52**, 045003 (2010).
[7] A. Murakami *et al*., Plasma Fusion Res. **5**, S1032 (2010).
[8] A. Murakami *et al*., J. Plasma Fusion Res. SERIES **9**, 79 (2010).
[9] S. Sakakibara *et al*., Plasma Fusion Res. **1**, 003 (2006).
[10] Y. Narushima *et al*., Fusion Sci. Technol. **58**, 194 (2010).
[11] A. Isayama *et al*., Nucl. Fusion **47**, 773 (2007).